ЕРЕВАНСКИЙ ФИЗИЧЕСКИЙ ИНСТИТУТ

PREPRINT YERPHI-1492(9)-97 (1997)

ՏՐՎԱԾՆԻ ՖԻԶԻԿԱՅԻ ԻՆՍՏԻՏՈՒՏ
ЕРЕВАНСКИЙ ФИЗИЧЕСКИЙ ИНСТИТУТ
YEREVAN PHYSICS INSTITUTE

Timing and Positioning Characteristics of a Fission Fragment Detector Based on Low Pressure Multiwire Proportional Chambers

G. Bavatyan, K. Egiyan, N. Grigoryan, S. Knyazyan, A. Margaryan, G. Merkyan, H. Mkrtchyan, L. Parlakyan, V. Tadevosyan, G. Vartanyan

Yerevan Physics Institute,
2 Alikhanian Brothers St., 375036 Yerevan, Armenia

N. Hamamyan, K.Baker, T.Eden, P.Gueye, C.Keppel, R.Madey, L.Tang

Department of Physics,
Hampton University, Hampton, VA 23668, USA

K.Cecire, P.Ent, H.Fenker, S.Majewski

TJNAF,
12000 Jefferson Ave, Newport News, VA 23606, USA

M.Planas, Z.Greenwood, K.Johnston, S.Wells

Department of Physics,
Louisiana Tech University, Ruston, LA, USA

C.J.Martoff

Department of Physics,
Temple University, Philadelphia, PA 19122, USA

S.Dumanoglian, R.Sawafta

Department of Physics,
North Carolina AT State University, NC, USA

Yerevan – 1998

Abstract

Results from investigations of timing and positioning characteristics of low-pressure multiwire proportional chambers (MWPCs) and multistep chambers (MSCs) are presented. Resolutions of about 170 ps full width at half-maximum (FWHM) for timing and .3mm (FWHM) for positioning were obtained by using low pressure MWPCs and MSCs, respectively, at the Yerevan Physics Institute. A time-zero fission fragment (FF) detector is proposed based on this low-pressure technique. The parameters of the FF detector are investigated by means of a Monte Carlo simulation, taking into account timing and positioning resolutions of low-pressure chambers, as well as physical processes that occur in the target and in the gas of the chamber. It is shown that time resolutions of better than 200 ps (FWHM) and zero-time scale accuracy of about a picosecond can be achieved.

1. Introduction

The utilization of nuclear fission as a reaction filter for the dynamics of low to intermediate energy nucleus-nucleus collisions has been widely exploited [1]. Recently it was shown [2] that fission can be used also as a filter for the study of heavy hypernuclei, and other exotic atoms and nuclei. In these kinds of experiments, one needs to detect unambiguously the fission fragments, measure their velocities, folding angles and energies. In some investigations, *e.g.*, for the direct measurement of heavy hypernuclei lifetimes [3], it is necessary to have a time-zero fission fragment detector. The properties of low-pressure multiwire proportional chambers (LPMWPCs) or multistep chambers (LPMSCs) [4] are very suitable for these goals . Among the qualities are the following:

1. Good timing resolutions ($\sigma \leq 50$ ps).
2. High efficiency for detecting fission fragments ($\sim 100\%$).
3. An extreme insensitivity to γ and neutron backgrounds.
4. High rate capability (count rates up to 10^5/ mm^2).
5. Negligible radiation damage.

This technique already has been used in experiments with heavy ions [5] and for the investigation of fission processes [6, 7, 8, 9, 10].

In this paper we present the timing and positioning characteristics of low-pressure techniques developed at the Yerevan Physics Institute [11,12], which have been investigated by means of a spontaneous source for fission fragments from ^{252}Cf and α- particles from ^{239}Pu. Finally, the parameters of time-zero fission fragment detectors, which consist of two pairs of LPMWPCs, are investigated by means of a Monte Carlo simulation, taking into account timing and position resolutions of low pressure chambers, as well as physical processes that occur in the target and in the gas of the chamber.

2. The Principle of the Low-Pressure Detector

a.) The LPMWPC.

The LPMWPC is a proportional counter with thre electrodes (two cathodes and one anode) having parallel-plane symmetry. The operational mechanism of the LPMWPC combines the principles of a regular multiwire proportional chamber (MWPC) and a parallel-plate avalanche counter (PPAC).

MWPCs [13] operating at normal gas pressures were never considered as time measuring devices, the reason being that their time resolution is of several tens of nanoseconds. This deficiency is due to the long drift time of electrons, released in the sensitive volume towards the sense wire where amplification occurs (Fig.1[a]). First measurements at low pressures (3 Torr) have shown that time resolutions of 2.5 ns (FWHM) could be reached with 5.5 MeV α-particles [14]. This result was simply attributed to a faster drift time at higher reduced fields. Further investigations [15,4] have clearly shown that the amplification mechanism at low pressures is entirely different (Fig.1[b]). The reduced electric field strength E/P in the constant region reaches values of several hundreds of V/cm · Torr which are very close to those reached in PPACs . PPACs are gas filled counters with two planar electrodes

(one cathode and one anode) operating in the proportional region which serves predominantly as time-sensitive detectors.

Primary electrons in a PPAC are accelerated by the strong uniform electric field ($E \sim 150$V/mm) between the electrodes, which causes ionization of additional atoms in the gas. Successive ionizations will result in the formation of a so-called Townsend-avalanche [16]. The electron multiplication in this constant field is an exponential function of the distance d, described by the Townsend formulae:

$$N(d) = N(0) \cdot e^{\alpha \cdot d}$$

Here $N(d)$ is the number of electrons after a drift distance d, α is the first Townsend coefficient, which is a function of the "reduced electric field" E/P, where P is the pressure inside the detector:

$$\alpha = P \cdot A \cdot \exp[-B/(E/P)]$$

The coefficients A and B are empirically obtained coefficients [16]: From the values measured by Breskin et al. [4], α in our case is estimated to be 30 cm^{-1}, corresponding to a mean-free path for ionization of 0.3 mm. A primary electron created at the cathode is multiplied by $e^9 \approx 8000$ times before reaching the vicinity of the wire. Close to the wire, the field strength increases strongly, leading to an effective electron multiplication in the vicinity of the wire.

The contribution of each part of the detector, the wires, and the constant field region, to the total gains have been studied [4] by comparing the gain of the MWPC with that of a PPAC, having a gap equal to the length of the constant field region of the MWPC, calculated according to Erskine's relation [17]. It has been clearly shown that higher gains are reached with the MWPC. The amplification factor of the wires vary from 5 to 2000, according to the gap and the pressure. The bulk of the electrons are therefore generated in a distance $1/\alpha$ in front of the anode, and the rise-time T_e of the electronic component of the signal is approximately the drift-time of these electrons across the last-mean ionization length $1/\alpha$:

$$T_e = \frac{(1/\alpha)}{V_e}$$

with $V_e = V_e(E/P)$ being the drift velocity of the electrons. Assuming $V_e = 5$ cm/μs, one gets $T_e \sim 7$ ns. Most of tese final secondary electrons stem from primary electrons created near the cathode. The time spread is reduced considerably and depends on the development of the Townsend-avalanche. Time resolutions on the order of 100 ps (FWHM) can be reached under these conditions.

Consider a "typical" fission fragment,^{115}Ag, traversing the detector with a velocity of 1.0 cm/ns. The stopping power of such a particle in isobutane at a pressure of 3 Torr is about 0.7 MeV/cm [18]. The effective ionization energy of isobutane is 23 eV [19] so about 3×10^4 primary electron-ion pairs/cm will be created. Assuming that only those electrons within 0.3 mm of the cathode are multiplied with a gain of about 10^5, 10^8 secondary electrons reach the wire. As a result a voltage drop on the order of 50 mV is expected from these counters.

During the amplification stage, the growing electron cloud expands and reaches a lateral size of about 1-2 mm (FWHM), depending on the gas pressure [4]; therefore, contrary to normal-pressure operation, the avalanche is not confined to a single wire, but is spread over several of them. This allows for good position interpolation between neighboring wires, while measuring charges induced on cathode wires or strips, connected to commercially tapped delay lines. A resolution of about 100 μm (FWHM) was obtained with fission fragments for an 80 cm^2 detector [20].

b.) LPMSC.

Multi-step avalanche chambers [21] are based on the preamplification of an initial charge and the transfer of the primary avalanche to a second stage for further amplification for a position or time measurement. Such detectors have been shown to be successful detection devices at normal gas pressures for minimum ionizing particles at high counting rates due to the gating possibility on selected events [22]. At normal gas pressures, some binary gas mixtures allow for an extended photon-mediated avalanche formation from which an efficient transfer of the preamplified charge to a second amplifying stage can occur. At low pressures, electron diffusion leads to wide avalanches. An efficient multistep amplification process can therefore occur even in pure organic gases, such as in isobutane, hexane, *etc.*, at pressures of 2-20 Torr, with an increase in total gain of one to two orders of magnitude, as compared to a single step detector [23,24]. In addition to the high attainable gains, LPMSCs have excellent timing and imaging resolutions, as well as high-rate operation properties. In this mode, the final stage of amplification, in which the vast majority of electron-ion pairs are produced, is suppressed electronically except during the application of an external gating signal. In a typical fixed-target physics experiment, the gate could be derived from a trigger signal indicating that some other part of the apparatus detected an interesting event.

c.) Space Charge Limitation of the Proportional Regime.

Larger signals from proportional chambers can be obtained by raising the applied voltage; but as the voltage is raised, one finds that: 1) the strict proportionality between deposited ionization and the signal is lost; 2) further increases in voltage lead to sparking. For very close wire spacing, breakdown may even occur before the semi-proportional region is reached [13].

Hanna, Kirkwood, and Pontecorvo [25] observed that the output pulse from a cylindrical proportional chamber ceases to be strictly proportional to the initial ionization when the absolute value of the charge exceeds some critical value Q. They found that this would correspond to losing 10^8 eV in the gas of the counter if there were no amplification, or to the creation of 5×10^6 ion pairs. Thus the upper limit on the amplification for proportional operation was $10^8/E$, where E is the energy in electron volts lost by the primary event. This type of limit can be understood as being due to a space-charge effect. For the "typical" fission fragment,^{115}Ag, traversing the detector with isobutane gas at a pressure 3 Torr, the upper limit on the amplification for proportional operation is about 5×10^3. In this case we have a voltage drop of 2.5 mV from the counters.

3. Experimental Investigation Timing and Positioning of LPMWPC

a.) Detector Design and Fabrication.

The present study was performed with LPMWPCs at Yerevan Physics Institute [11,12]. These circular MWPCs, 60 mm in diameter, are presented schematically in Fig. 2. Each MWPC has three planes, two cathode and one anode. The wire planes are made of parallel and equidistant wires. The wire spacing is 1 mm, the distance between an anode and cathode plane is 3 mm. Different kinds of wire (gold-plated tungsten, beryllium bronze) with different diameter thicknesses (10, 20, 50, 100 μm) have been used. The circular frames of the detector, mounted in a stainless steel or aluminum vacuum tight vessel, are shown in Fig. 3. The detector vessel is sealed with viton O-rings. It is coupled to a vacuum pumping system and can be evacuated to a pressure of 10^{-3} Torr. The vessel is equipped with stainless steel valves for gas handling and with two barometers. One of the barometers was used to measure the vacuum level in the vessel; the second one was used to measure the gas pressure. The chamber volume, connected to a reservoir of liquid hexane or heptane with a reducing valve, was filled with 1-5 Torr of hexane or heptane vapors. A pressure range of 1-2 Torr turned out to be optimal for timing of fission fragments. Investigations were performed with a ^{252}Cf deposited on a 50-μm Aluminum foil. The fission source was placed in the front of the FF counters. The source and the first detector were separated by a distance of 30 mm. The 50-μm thick Mylar collimator, with a circular hole, was mounted between the source and the FF counters to decrease the path length fluctuations of the FF. The diameter of the hole and the distance from the ^{252}Cf source were 16 mm and 17 mm, respectively.

b.) Timing Characteristics of LPMWPC.

The timing properties of an LPMWPC were studied using two MWPCs placed next to each other at a distance of 9 mm in a common gas container. The time difference between the two detectors was measured using fast preamplifiers [26], constant-fraction discriminators, time-to-amplitude converters, and a multichannel analyzer. A simplified scheme for the geometry and electronics for timing investigations are presented in Fig. 4. An example of the time difference spectra is presented in Fig. 5. The time scale was determined by adding a calibrated delay to the output of one of the constant fractions. The FWHM of the total time resolution is $\Delta t = 530$ ps for an applied voltage of 430 V. Because the start and stop detectors contribute equally to the time resolution, the time resolution for one detector is reduced by a factor of $\sqrt{2}$; therefore, the total time resolution for one detector is 375 ps.

The measured time resolution Δt_{eff} is composed of different contributions: 1) a kinematic part Δt_{kin} due to different fragment velocities within the light or heavy fragment mass distribution; 2) a geometric part Δt_{geom} due to the difference in flight paths between detector-1 and detector-2 ; 3) an electronic time jitter Δt_{el}; 4) an intrinsic part Δt_{intr} caused by statistical fluctuations in the drift time of the avalanches. Since the last two terms are about the same for both chambers and

uncorrelated, we have:

$$(\Delta t)^2_{eff} = (\Delta t_{kin})^2 + (\Delta t_{geom})^2 + 2 \cdot [(\Delta t_{el})^2 + (\Delta t_{int})^2)]$$

The kinematic and geometric contributions can be calculated using the well known energy distributions of ^{252}Cf fission fragments [27]. The electronic time jitter in this measurement was about 150 ps. The estimated intrinsic time resolution of one detector is about 200 ps. The dominant contribution to Δt_{eff} are the kinematic and geometric parts.

To decrease the kinematic and geometric parts in the time difference spectrum between detector-1 and detector-2, we use a third FF counter located in the same gas container at a distance of 66 mm from detector-2. The time difference spectrum between detector-1 and detector-3 is displayed in Fig. 6. Again, contributions to the spectrum come from different mechanisms such as, kinematic, geometric, and electronic and intrinsic resolutions of the detectors. The dominant contribution to the Δt_{eff} from the kinematical and geometrical parts is proportional to the distance between detector-1 and detector-3; and in Fig. 6, the time-spectrum of the light and heavy fragments of a ^{252}Cf source are well separated.

We use signals corresponding to the light fragments as a gate for the time difference spectrum between detector-1 and detector-2. By means of this gate, we select the fragments with a small time difference Δt_{13} between detector-1 and detector-3. The time difference Δt_{12} between detector-1 and detector-2 for these fragments due to kinematical and geometrical mechanisms is:

$$\frac{\Delta t_{12}}{\Delta t_{13}} = \frac{9}{75}$$

Therefore, we can practically avoid the kinematic and geometric factors in the time difference distributions of detector-1 and detector-2. The simplified scheme of electronics for this timing measurement are shown in Fig. 4. The gated time difference between detector-1 and detector-2 is presented in Fig. 7[a,b]. The gate lengths for the time difference distributions presented in Figs. 7a and 7b correspond to 120 ps and 60 ps time differences between fragments at detector-3, respectively. The time distance between these two distributions is 2 ns. The time resolutions (FWHM) are 350 and 340 ps for the first and second cases, respectively. The estimated pure intrinsic and electronic time resolution (FWHM) for a zero gate length is:

$$\left[2 \cdot ((\Delta t_{el})^2 + (\Delta t_{int})^2)\right]^{1/2} = 330\text{ps}$$

For $\Delta t_{el} = 150$ ps, we have $\Delta t_{int} = 170$ ps.

As was reported earlier [4], for counting rates as high as 5×10^4 c/s$\cdot$ mm^2, the time resolution of an LPMWPC is not affected.

We studied the influence of high background α-particles for the FF timing resolution of LPMWPCs. The presence of an intense and nonmonochromatic α source (about 2×10^5/sec), does not affect the time difference spectrum of detector-1 and detector-2, which measured with the help of a fission fragment rate of a few fragments/sec. The efficiency for detecting α-particles is $\leq 10^{-4}$. The resulting time difference spectrum is shown in Fig. 8.

c.) Position Resolution.

When an avalanche occurs on an anode wire, a positive charge is induced on the cathodes. The position of the avalanche can be determined by measuring the center of gravity of the induced charge distribution using various methods such as delay lines, charge-division, or direct computation.

We investigated the localization capabilities of low-pressure MSCs using delay lines [28,29]. Position sensing with delay lines is based on conversion of position information into a time delay. In this method, position sensing electrodes in the detector are connected at a uniform spacing to a delay line. The signal can be coupled either capacitively, or directly. If cathodes of a multiwire proportional chamber are connected to the delay line, a well known interpolating property results [28]. The image of the signal charge is seen by several electrodes, and by determining the centroid of the composite signal propagating along the delay line, the position can be determined with an error smaller than the wire spacing.

In principle, the delay line is a non-dissipative position sensing medium. The noise in this system is generated in the termination of the signal and in the amplifiers. The position resolution is ultimately limited by the statistics of the spatial charge distribution in the detector. The electronic noise determines the magnitude of the signal required to achieve this resolution.

The relative position resolution is determined by the timing error from the two outputs. The noise from the two outputs is uncorrelated for timing, thus:

$$\frac{\Delta x}{x} = \sqrt{2} \cdot \frac{\Delta t}{t}$$

The gas gain of an LPMSC is higher than the gain of an LPMWPC. Due to this gain difference, the localization capabilities of the LPMSC can be investigated by means of an available intense α-particle source. For this reason, we carried out position investigations using the MSC configuration with the low-pressure technique. The planes of the MSC also have a circular form, with a diameter equal to 60 mm, having golded-tungsten 12.5 μm thick anode wires 1 mm apart. The gap between the anode and cathode is 3 mm. The cathodes are made of 90-μm-thick Beryllium-Bronze wires, spaced 1 mm apart. Using Beryllium-Bronze wires allows one to increase the anode voltages up to 500 V. The signals from α-particles were about 5-10 mV and the preamplification gap was 3 mm. The three cathode wires were connected together to the taps of the delay-line chips. The delay-line chips of the type 1507-20B (Data Delay Devices, inc.) having a delay of 2 ns between taps and a impedance of 100 Ohms was used. The position of the avalanche was obtained by measuring the time difference between the induced pulses propagating towards the two ends of the delay lines. Low-noise preamplifiers and constant fraction timing discriminators were used to process the signals. A schematic of the electronics is shown in Fig. 9. At first, we carried out the measurement for linearity of the delay-line chips. The results of such a measurement, for two delay-line chips connected successively, are shown in Fig. 10. In general, linearity is observed; but for accurate position determination, absolute calibration using a well collimated source is necessary. The attenuation coefficient of signals traversing through one delay-line chip (20 ns) is

0.95. The position of the avalanche is obtained by measuring the time difference between the induced pulses propagating towards the two ends of the delay line, as shown in Fig. 9. Position resolutions were measured at 2 Torr of hexane with α particles from ^{239}Pu. A collimator, made of .05mm slits, was placed at a distance of 28.4 mm from the detector; their image on the anode of the detector was .32 mm. The center to center distance between slits is 5.8 mm. Figure 11 shows the position distribution of the collimated source. The resolution of each peak is .44mm (FWHM). The estimated intrinsic position resolution of the chambers is on the order of .3mm (FWHM).

The position can be determined also by measuring the time difference between the anode and one of the induced pulses. In this case we obtain a .6mm resolution, instead of .3mm.

4. Time-Zero Fission Fragment Detector

Good timing and positioning parameters for the low-pressure technique allows for one to develop a time-zero fission fragment detector, *i.e.* a detector, which permits measuring the fission time of nuclei in a target. Such a detector can be used for the direct measurement of heavy hypernuclei liftimes at TJNAF [3]. The proposed design of the time-zero FF detector is shown in Fig. 12. The FF detector consists of two pairs of low-pressure chambers. The first chamber is placed at a distance of 3 cm from the target. The distance between the first and second chamber is 7 cm. The signals from the anodes and cathodes will be used for time and position measurements, respectively. The fine beam micro structure at CEBAF and other electron accelerators provides beam bunch timing of nearly zero width. Furthermore, the beam bunch time t_0^b is practically equal to the production time of a nuclear reaction. Each chamber in the FF detector system will record a time t_i after a Δt_{FF} time of flight of fission fragments. For prompt fission events:

$$t_0^p = t_i - \Delta t_{FF}.$$

For delayed fission events:

$$t_0^d = t_i - \Delta t_{FF} + \Delta t_d,$$

where Δt_d is the decay time.

By means of a FF detector, we will measure the velocities and reconstruct tracks of fission fragments which will allow us to determine experimentally event by event the fission fragment production time-t_0. In an ideal case for prompt fission, the distribution f_p of the measured t_0^p must be Gaussian like with a mean value equal to 0. With out experimental error, the distribution f_d of t_0^d for delayed fission will look like an exponential with the decay constant equal to the lifetime τ_Λ. The distribution f_d of the measured T_0^d will be a convolution of the experimental resolution function r and the probability density f:

$$f_d(t, \tau_\Lambda) = \int f(t - t', \tau_\Lambda) r(t') dt'$$

A three-dimensional Monte Carlo (MC) code was developed for the investigation on the influence of physical processes connected with the penetration of fission fragments through the target and the gas chamber, to the time characteristics of a FF

detector, taking into account the timing and position characteristics of low-pressure chambers. For the resolution (FWHM) of timing and position for each chamber of the FF detector, we take the experimentally obtained results 235 ps and .3mm, respectively.

The penetration of fission fragments through the target is simulated, taking into account the ionization energy loss, charge-exchange, and multiple scattering processes. The theoretical description of the stopping power for fission fragments is more difficult than for elementary particles, because the fragments both lose and gain electrons during their passage through matter; therefore, the excitation spectrum is calculated for each single charge state q. The mean energy loss ΔE of the fragment in ΔX_i is then:

$$\Delta E = S_p \times \Delta X_i \times \sum_{q=1}^{q=Z_F} q^2 \phi(q, v_F)$$

where $\phi(q, v_F)$ is the charge state of the equilibrum distribution and

$$q_{eff}(v_F) = \left[\sum_{q=1}^{q=Z_F} q^2 \phi(q, v_F) \right]^{1/2}$$

is the so called effective charge of the fragment, and S_p is the stopping power of protons for the same velocity. For q_{eff}/Z_F, we use the following expression [30]:

$$q_{eff}/Z_F = 1. - 1.034 \times \exp[-v_F/(v_0 \cdot Z_F^{0.648})]$$

where Z_F is the charge of the fragment, and $v_0 = 2.19 \times 10^8$(cm/sec) is the Bohr velocity. We assume charge equilibrum distribution is Gaussian like with $\sigma = .115 \times (Z_F)^{1/2}$.

For the calculation of S_p, we use the oscillator model with shell corrections [31,32]. For multiple scattering, the Moliere theory developed for thin layers of matter [33] was used. In order to reduce the computation time, the transport of fission fragments in the target is modeled by the method of "group" collisions [34]. According to this method, the ranges of fragments in the target is divided into steps ΔX_i. In the case of a Bi target the steps are $\Delta X_i = 10^{-5}$ cm. It is assumed that within each step, the fragment track is a straight line. Ionization energy loss occurs only during a transition from one step to the next, while the fragment undergoes scattering, as well as changes in charge state due to multiple scattering and charge-exchange processes. The fragments are followed in the target until they stop or escape the target. If the fragment emerges from one of the two surfaces of the target, the motion is then considered in the gaseous medium. The fission fragments are considered to be stopped, if their energy becomes less than 2 MeV.

The transport of fission fragments in the gaseous medium is simulated by a different method. In this case, the energy loss and charge-exchange processes were considered only. The track of the FF is divided into parts about a millimeter in length. It is assumed that within each step, the fragment charge is a constant. Charge states of the fission fragments are changing during transition from one step

to the next. Ionization energy losses occur continuously by the help of the individual collission model [31].

The mass distribution of fragments is sampled from a Gaussian like distribution with a width (FWHM) equal to 56 atomic mass units [35], corresponding to a symmetric fission mode. The charge to mass number ratio of fission fragments was taken to be the same as the fissioning nucleus [36]. Kinetic energy of fragments was determined by the help of Viola systematics [1], assuming that the mass and charge of the compound nuclei are the same as for Bi.

The Monte Carlo time difference spectrum between two chambers, situated according to the geometry of Fig. 4, is shown in Fig. 13. For comparison, the experimental data are shown as well. There is good agreement between the MC and the experimental spectra. In Fig. 14, the MC distribution f_p of the t_0^p for only one(first) plane, when fragments enter perpendicularly to the chamber plane of the detector is shown. In an ideal case, the average value of the t_0^p must be equal to 0. Calculations were done with and without gas in the chamber. The f_t distribution, without a gas environment, is Gaussian-like with a mean value of 1 ps. The existence of the gas environment influences the time distribution. In the case of heptane at a pressure of 1 Torr, the mean value of the T_0^p distribution is on the order of 100 ps. This phenomenon must be taken into account in the TJNAF E95-002 experiment; the main goal of which is the direct measurement of the lifetime of a delayed fission process. The delayed fission in this experiment is associated with the heavy hypernuclei production. The expected lifetime of heavy hypernuclei is on the order of 100 ps; therefore, the influence of the energy loss to fragments velocities in the gas of the chamber, can mask the effect and/or to serve as a source of systematic error. The abundant number of prompt fission events and the MC code will be used continuosly for appropriate calibration of the fission-fragment detector. However, the distribution of the mean time-zero of all four planes is more Gaussian like, and 200 ps delayed fission events are slightly different, as shown in Fig.15. The mean values for these time difference spectra are 24 ps and 225 ps, respectively. Their difference is equal to the lifetime of the delayed fission. Fitting the obtained lifetime spectrum of 10^3 events by the convolution of the resolution function with an exponential decay, using a fitting algorithm based on Gaussian statistics, the hypernuclear lifetimes can be determined with a good precision ($\leq 5\%$).

A detailed description of the present MC code will be presented in a different paper.

4. Summary

Resolutions of about 170 ps (FWHM) for timing with fission fragments from ^{252}Cf and .3mm (FWHM) for positioning with α-particles from ^{239}Pu have been obtained using LPMWPCs and LPMSCs, respectively.

Based on these techniques time-zero fission fragment detectors, are proposed. The characteristics of such a detector were investigated with the help of a Monte Carlo simulation, taking into account timing and position resolutions of low pressure chambers, as well as physical processes connected with fission and with penetration of fission fragments through the target and gaseous medium of the chambers. Because of the small thickness of the target($\sim 2\mu$m), energy loss and straggling of fragments in the target are not noticeable; notwithstanding, the fragments lose about half of their kinetic energy in the target; in contrast, a minor energy loss of fragments in the gas of the chamber even at pressure of 1 Torr, influences slightly the shape of the time distribution of the proposed time-zero detector. This phenomenon, which can become a source of systematic error in delayed fission lifetime measurement experiments, can be controlled with the help of appropriate calibration techniques using abundant prompt fission events.

The proposed fission fragment detector can be employed for the investigation of the prompt and delayed fission processes as well as for the study of heavy hypernuclei and other exotic atoms and nuclei.

Acknowlegments

The work is supported in part by Grant Number YPI 211-5221 of the German Bundesministerium for Forschung und Technologie, by a Grant from the United States Civilian Research and Development Foundation (Award AP1–102), and by a Grant from the National Science Foundation HRD–9633750.

Figure Captions

Fig.1 Operation mechanism of MWPCs. (a) At normal gas pressures, electrons collected from the sensitive volume are amplified in the region of the wires. (b) At low pressures, electrons start an avalanch in the constant field region: a second amplification step occurs when the electron swarm reachs the wires.

Fig.2 Schematic drowing of the detector.

Fig.3 Schematic diagram of the gas handling system.

Fig.4 Schematic diagram of the geometry and electronics of timing investigations of LPMWPCs. PA - preamplifier, CFD - constant fraction discriminator, TAC - time to amplitude converter, DD - single channel analyzer, MCA - 1024 channel analyzer, DL - delay line.

Fig.5 TOF - spectrum of fragments from a ^{252}Cf source between LPMWPCs D1 and D2 (1 ch = 56 ps).

Fig.6 TOF - spectrum of fragments from a ^{252}Cf source between LPMWPCs D1 and D3 (1 ch = 140 ps).

Fig.7[a,b] Gated TOF-spectrum of fragments from a ^{252}Cf source between LPMWPCs D1 and D2 (1 ch = 84 ps). The gate widths are 120 ps (a) and 60ps (b), respectively. The separation between the two peaks in time is 2 ns.

Fig.8 TOF - spectrum of fragments from a ^{252}Cf source and α- particles from ^{239}Pu between LPMWPCs D1 and D2 (1 ch = 168 ps).

Fig.9 Simplified scheme of the electronics for positioning investigations of LPMWPCs. PA - preamplifier; CFD - constant fraction discriminator; DL - delay line; CA - 1024 channel analyzer; TAC - time to amplitude converter.

Fig.10 Relationship between the number of delay - line taps to the centroid of the delay - line time distribution.

Fig.11 Position resolution of the LPMSC measured at 2 Torr with α- particles and with a set of fine slits placed in front of the detector. The slit's image on the anode plane is .32mm. The intrinsic resolution is .3mm (FWHM). The distance between the two peaks is 5.8mm.

Fig.12 A schematic sketch of the time - zero FF detector.

Fig.13 TOF - spectrum of fragments from a ^{252}Cf source between LPMWPCs D1 and D2 (1 ch = 112 ps). Shown are the results of the measurement (solid line) and Monte Carlo simulation (dashed line).

Fig.14 Monte Carlo time - zero distribution of fragments from Bi for the first chamber of time-zero FF detector (1ch = 100 ps). The curves belong to the cases without gas (solid line) and with Hexane at 1 Torr pressure (dashed line).

Fig.15 Monte Carlo time - zero distribution of fragments from Bi for the four chambers of the time-zero FF detector system (1ch = 100 ps). The curves belong to the cases of delayed fission with a 200 ps lifetime (dashed line) and with prompt fission (solid line).

References

[1] V.E. Viola, Nucl. Phys. **A502**(1989) 531C.

[2] A.T. Margarian, Nucl. Instr. and Meth. **A357** (1995) 495.

[3] TJNAF EXP95-002 "Direct Measurement of the Lifetime of Heavy Hypernuclei at CEBAF", L.Tang and A.Margarian (Cospokespersons)

[4] A. Breskin, R. Chechik, N. Zwang, IEEE Trans.Nucl.Sci.NS-27 (1980) 133.

[5] M. Overbeck *et al.*, Nucl. Instr. and Meth. **A288** (1990) 413.

[6] S. Polikanov *et al.*, Z. Phys., **A350** (1994) 221.

[7] E.A. Arakelian *et al.*, Sov. J. Nucl. Phys., **52** (5) (1990) 878.

[8] E.A. Arakelian *et al.*, Sov. J. Nucl. Phys., **49** (5) (1989) 780.

[9] E.A. Arakelian *et al.*, Sov. J. Nucl. Phys., **49** (6) (1989) 1022.

[10] E.A. Arakelian *et al.*, Phys. Atomic Nucl., **58** (1995) 219.

[11] E.A. Arakelian *et al.*, Prib. i Tekh. Eksp., **3** (1989) 68.

[12] E.A. Arakelian *et al.*, Nucl. Phys. B(Proc. Suppl.), **23A** (1991) 307.

[13] G. Charpak, Ann. Rev. Nucl. Sci., **20** (1970) 195.

[14] F. Binon *et al.*, Nucl. Inst. and Meth., **94** (1971) 27.

[15] A. Breskin *et al.*, Nucl. Inst. and Meth., **165** (1979) 125.

[16] H. Stelzer, Nucl. Instr. and Meth., **133** (1976) 409.

[17] G.A. Erskine, Nucl. Instr. and Meth., **105** (1972) 565.

[18] Stopping Power and Range of Ions in Matter, **vol. 6** edited by J. F. Ziegler, Pergamon Press, New York, 1980.

[19] F. Sauli, CERN Report 77-09, (1977)

[20] A. Breskin *et al.*, Nucl. Instr. and Meth.,**217** (1983) 107.

[21] A. Breskin *et al.*, Nucl. Instr. and Meth.,**161** (1979) 19.

[22] A. Breskin *et al.*, Nucl. Instr. and Meth.,**178** (1980) 11.

[23] A. Breskin, G. Charpak, S. Majewski, Nucl. Instr. and Meth.,**220** (1984) 349

[24] A. Breskin *et al.*, Nucl. Instr. and Meth .,**221** (1984) 363

[25] G.C. Hanna, D.H.W. Kirkwood and B. Pontecorvo, Phys. Rev. **75** (1949) 985.

[26] L. . Parlakian, Preprint YerPhi-1439(9)-95 , Yerevan (1995)

[27] H. '. Schmit, J.H. Neller and F.J. Walter, Phys. Rev. **141** (1966) 1146.

[28] R. Grove *et al.*, Nucl. Instr. and Meth., **89** (1970) 257.

[29] V. Radeka, IEEE Trans. on Nucl. Sci., **NS-21**, n.1 (1974) 51.

[30] M). Brown and C.D. Moak, Phys. Rev. **B6** (1972) 90.

[31] K . Ispirian *et al.*, Nucl. Instr. and Meth., **117** (1974) 125.

[32] R 'alman, Nucl. Instr. and Meth., **159** (1979) 189.

[33] A . Margarian, Scintific Report of YerPhI, EFI-431(38) 80, Yerevan (1980).

[34] A. . Margarian, Scintific Report of YerPhI, EFI-564(51)-82, Yerevan (1982).

[35] R Folger, P.C. Stevenson and G.T. Seaborg, Phys.Rev. **98** (1955) 107.

[36] R . Goeckermann and J. Perlman, Phys.Rev. **76** (1949) 628.

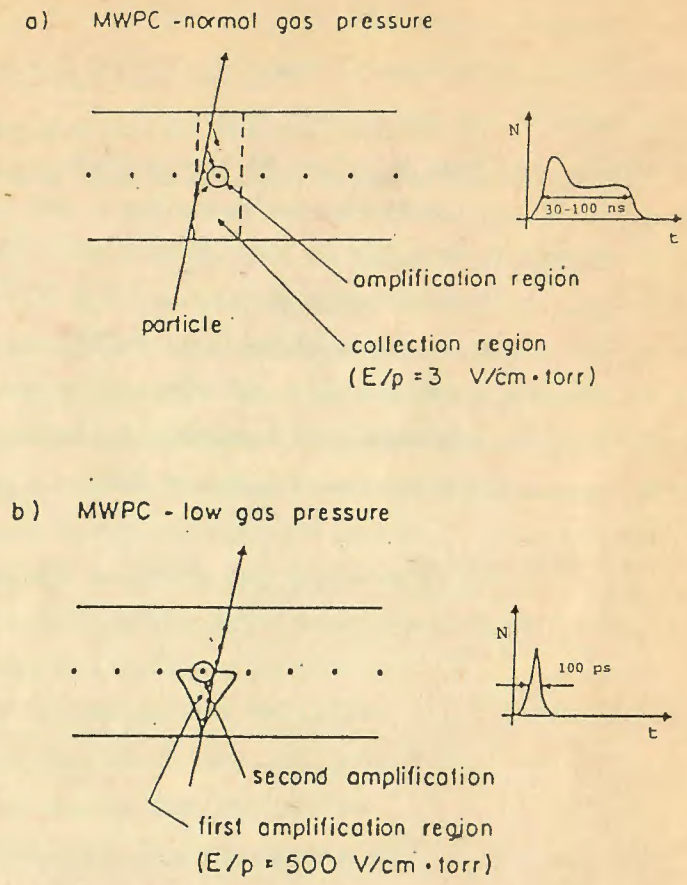

Fig.1 Operation mechanism of MWPCs.
(a) At normal gas pressures, electrons collected from the sensitive volume are amplified in the region of the wires.
(b) At low pressures, electrons start an avalanch in the constant field region: a second amplification step occurs when the electron swarm reaches the wires.

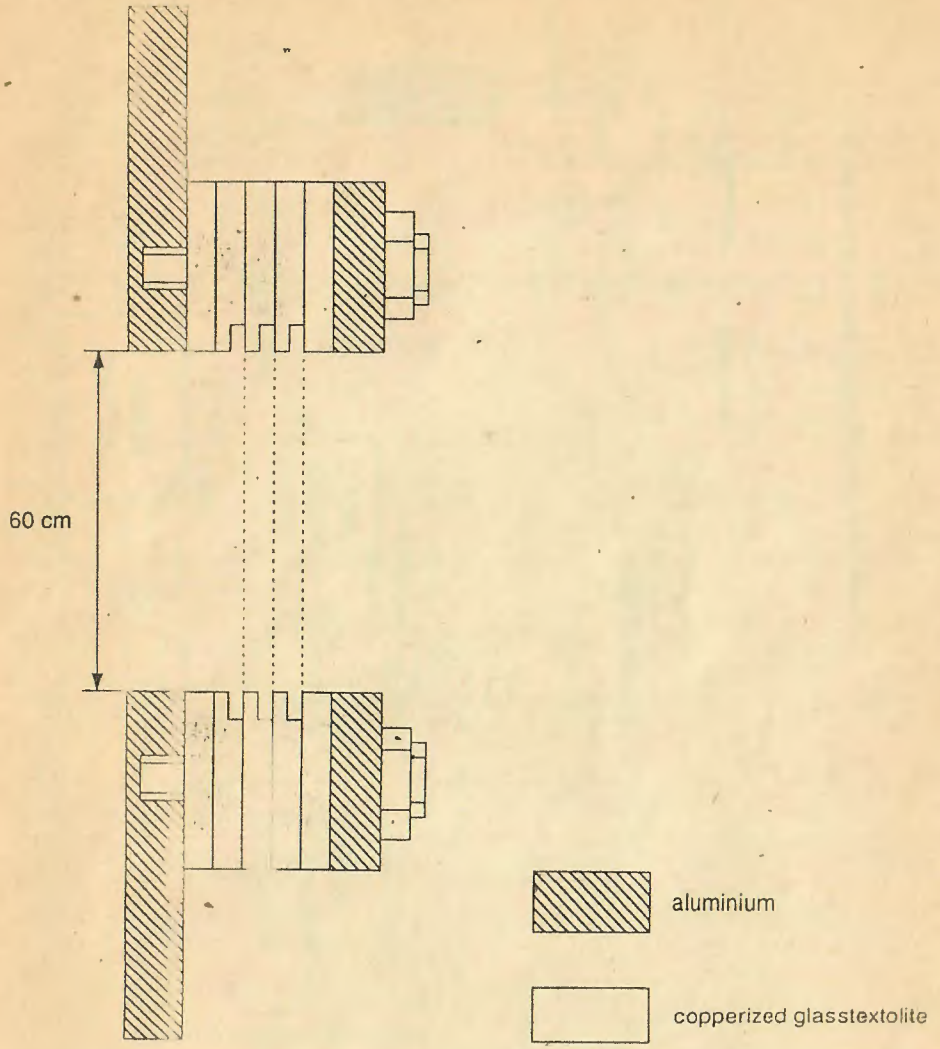

Fig.2. Schematic drawing of the used MWPC.

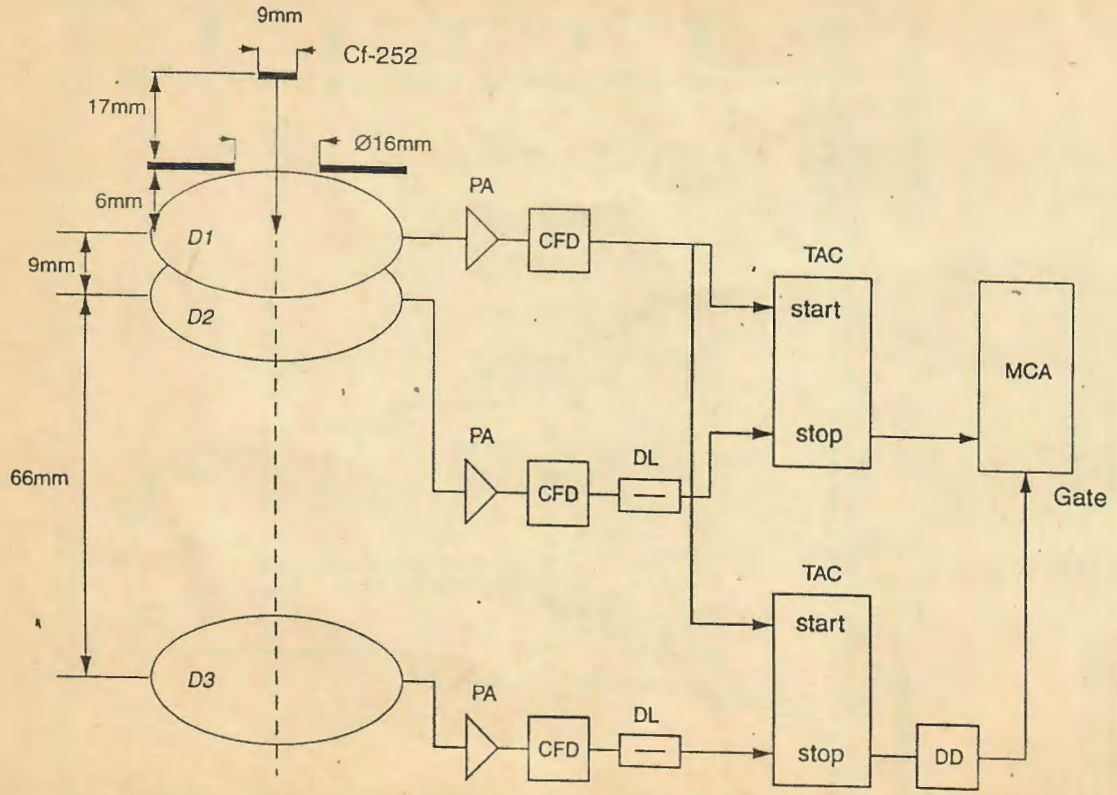

Fig.4 Schematic diagram of the geometry and electronics of timing investigations of LPMWPCs. PA - preamplifier, CFD - constant fraction discriminator, TAC - time to amplitude converter, DD - single channel analyzer, MCA - 1024 channel pulse analyzer, DL - delay line

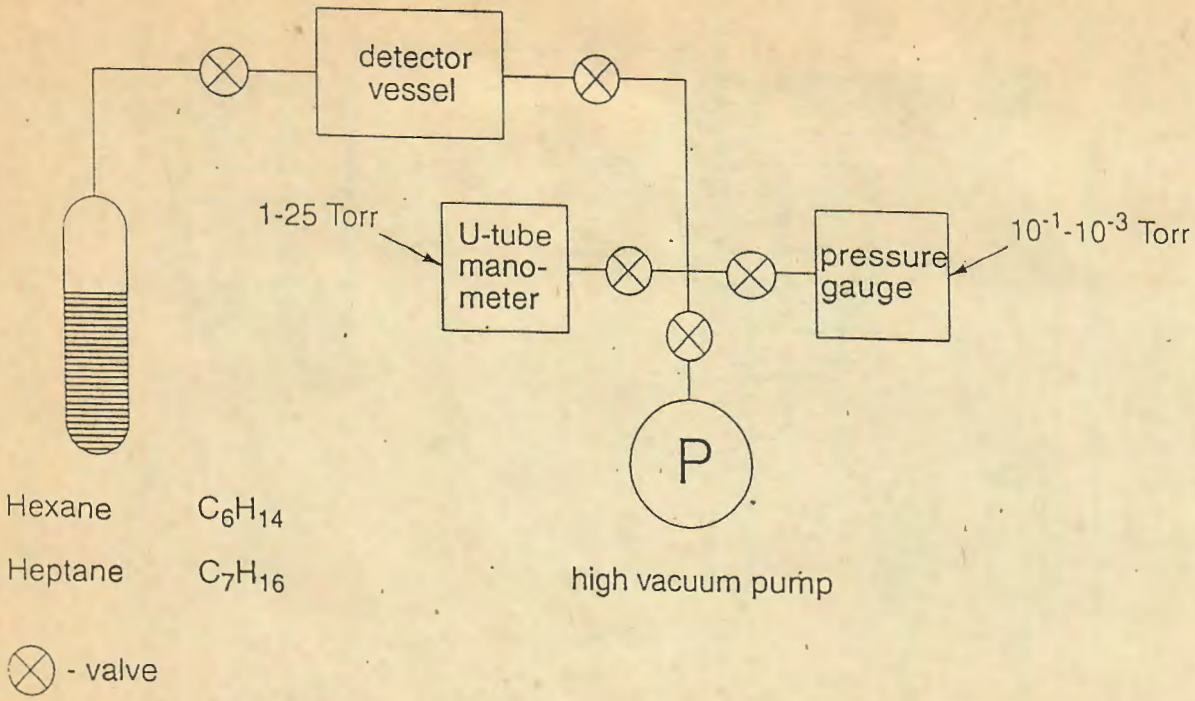

Fig.3 Schematic diagram of the gas handling system.

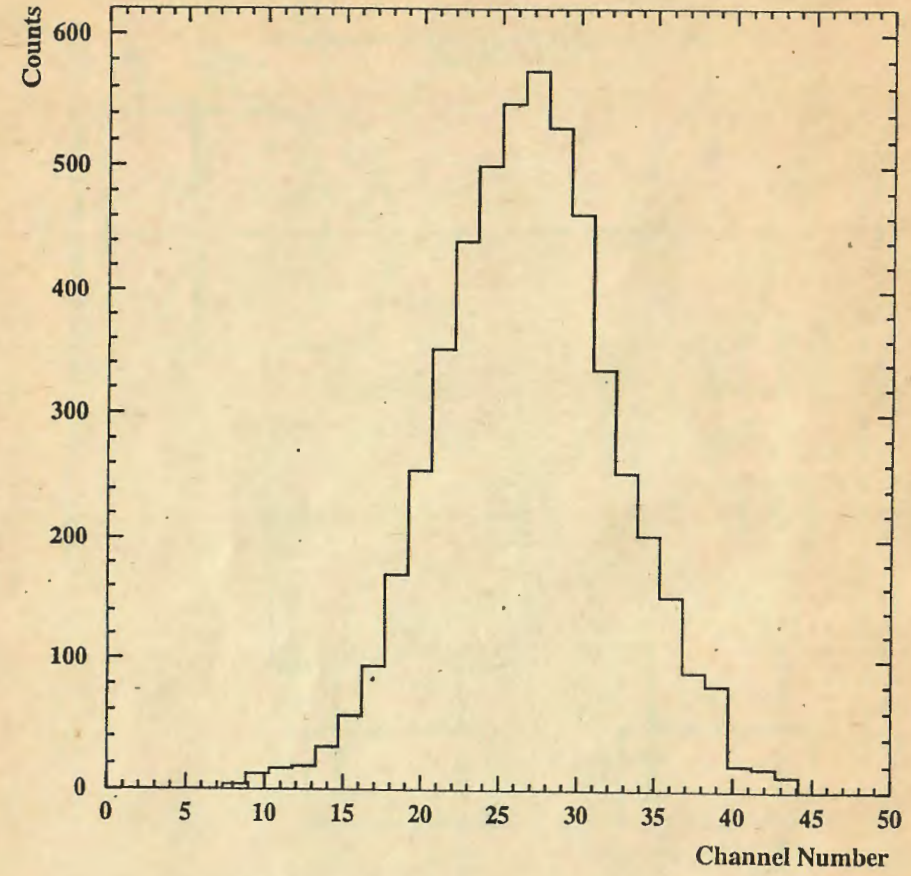

Fig.5 TOF-spectrum of fragments from a ^{252}Cf source between LPMWPCs D1 and D2 (1 ch = 56 ps).

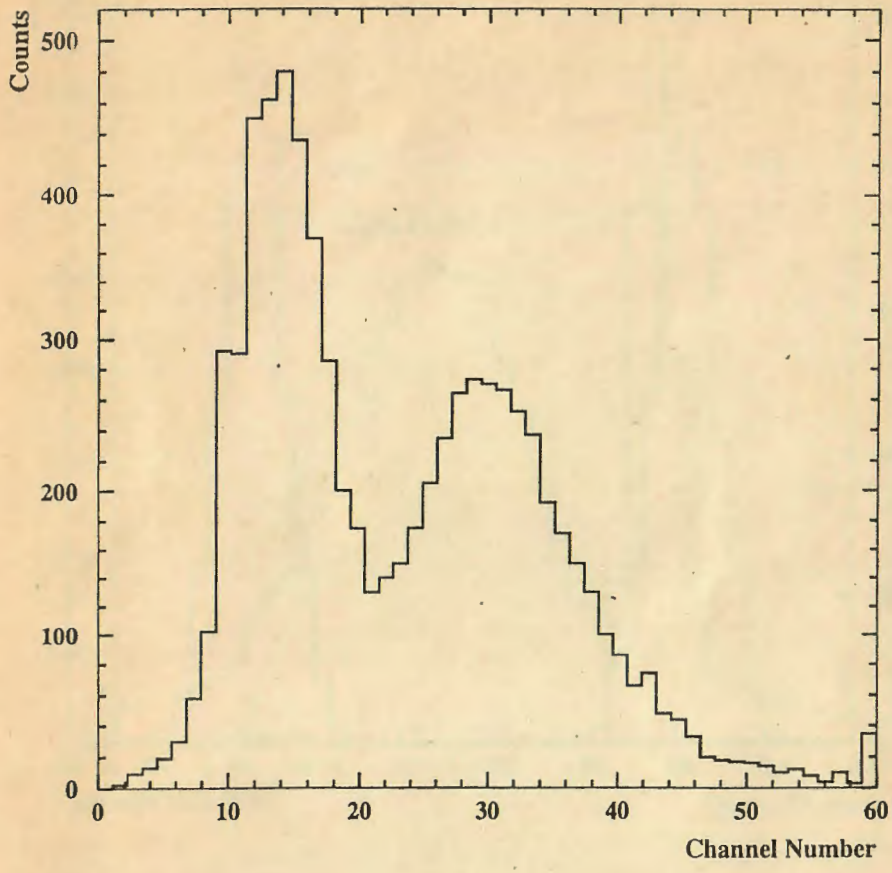

Fig.6 TOF-spectrum of fragments from a ^{252}Cf source between LPMWPCs D1 and D3 (1 ch = 140 ps).

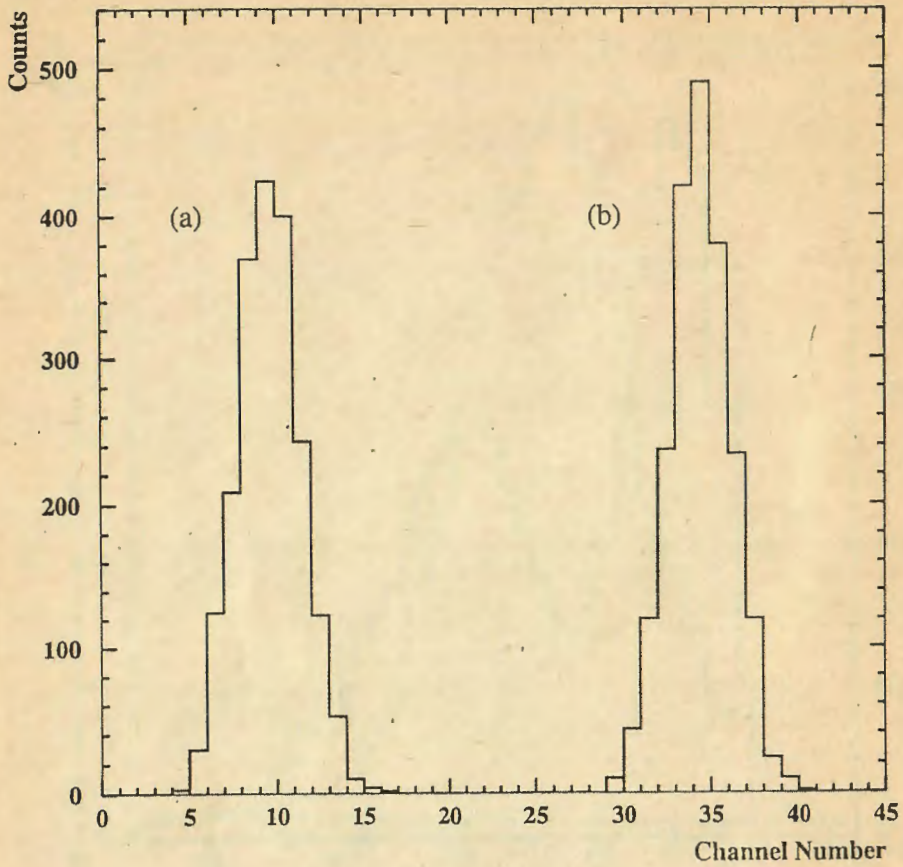

Fig.7[a,b] Gated TOF-spectrum of fragments from a ^{252}Cf source between LPMWPCs D1 and D2 (1 ch = 84 ps). The gate widths are 120 ps (a) and 60 ps (b), respectively. The separation between the two peaks in time is 2 ns.

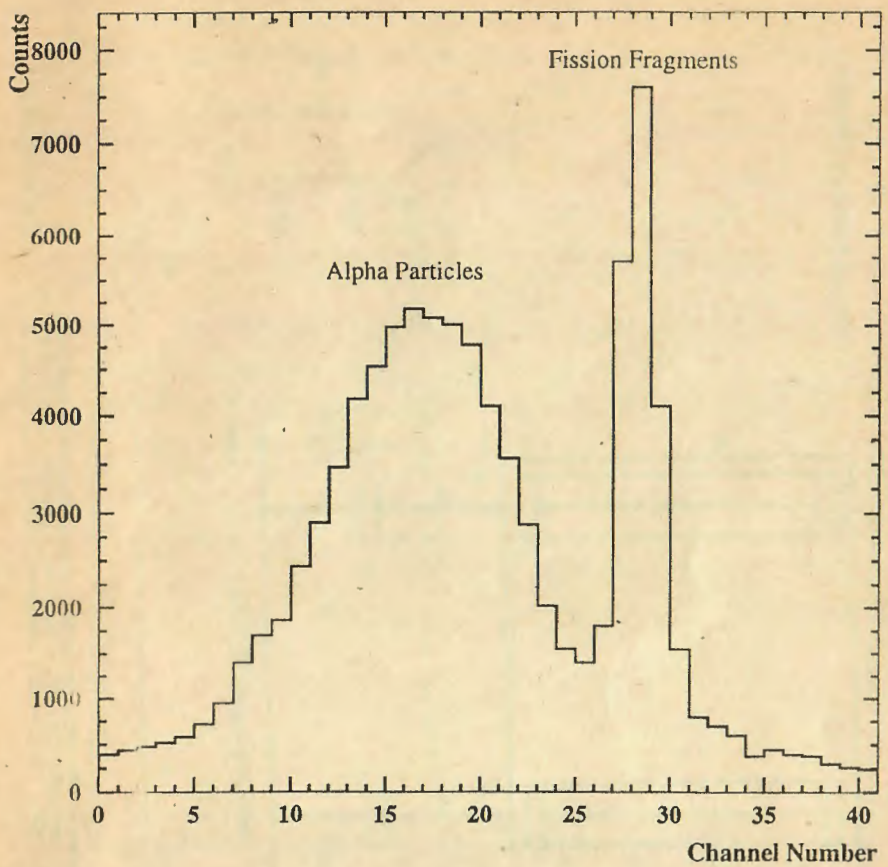

Fig.8 TOF-spectrum of fragments from a ^{252}Cf-sorce and alpha-particles from a ^{239}Pu between LPMWPCs D1 and D2 (1 ch = 168 ps).

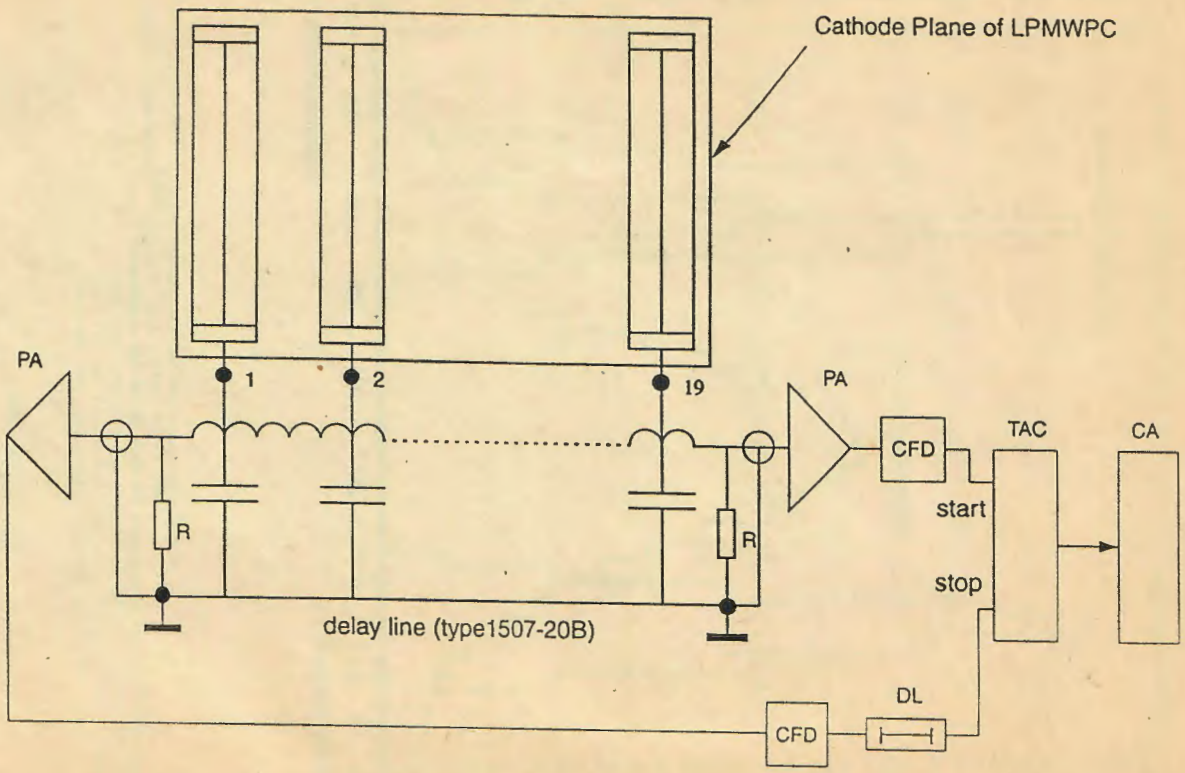

Fig.9 Simplified scheme of the electronics for positioning investigations of LPMSCs. PA - preamplifier; CFD - constant fraction discriminator; DL - delay line; CA - 1024 channel analyzer; TAC-time to amplitude converter.

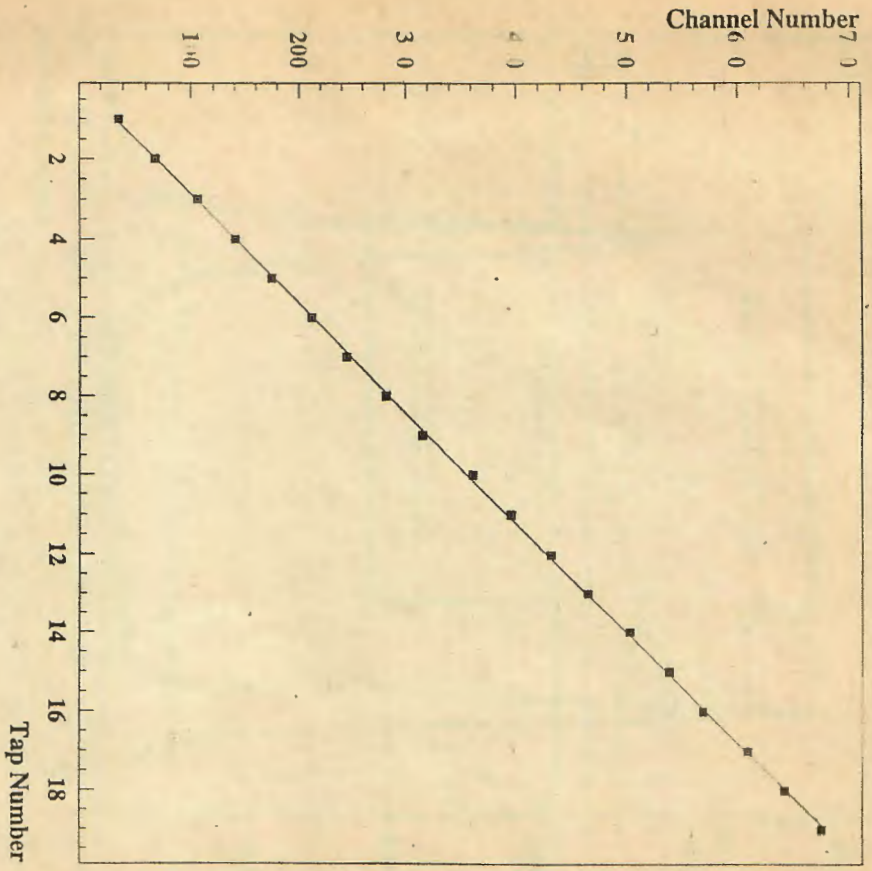

Fig.10 Relationship between the number of delay-line taps to the centroid of the delay-line time distribution.

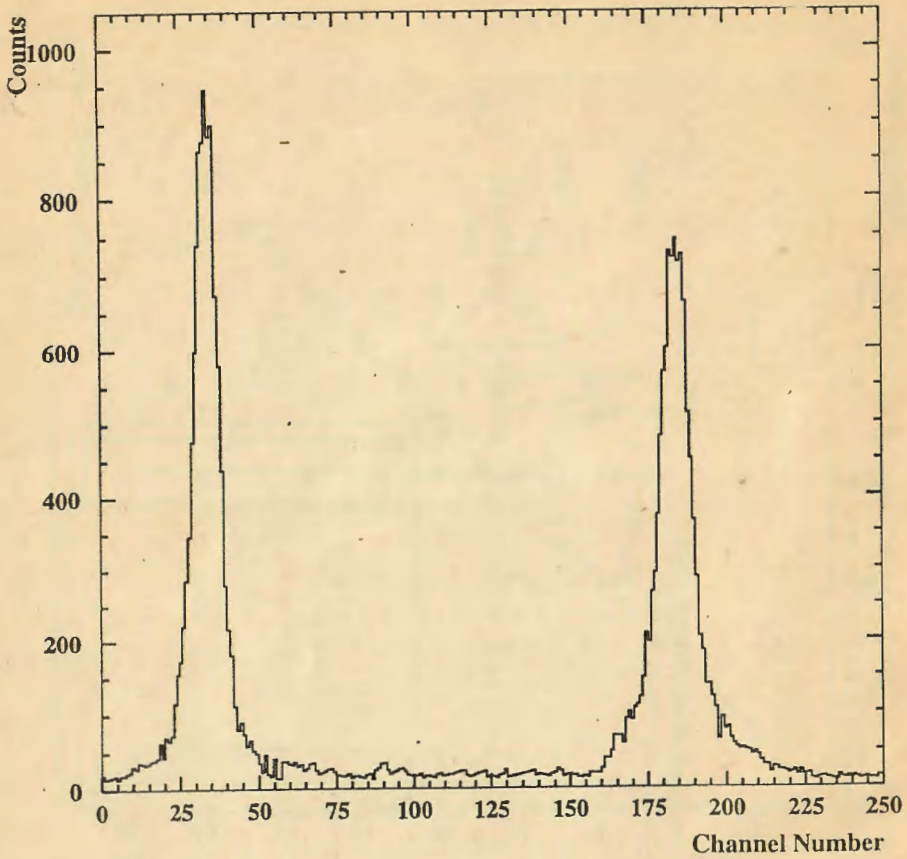

Fig.11 Position resolution of the LPMSC measured at 2 Torr with alpha-particles and with a set of fine slits placed in front of the detector. The slit's image on the anode plane is 320 μm. The intrinsic resolution is 300 μm (FWHM). The distance between the two peaks is 5.8 mm.

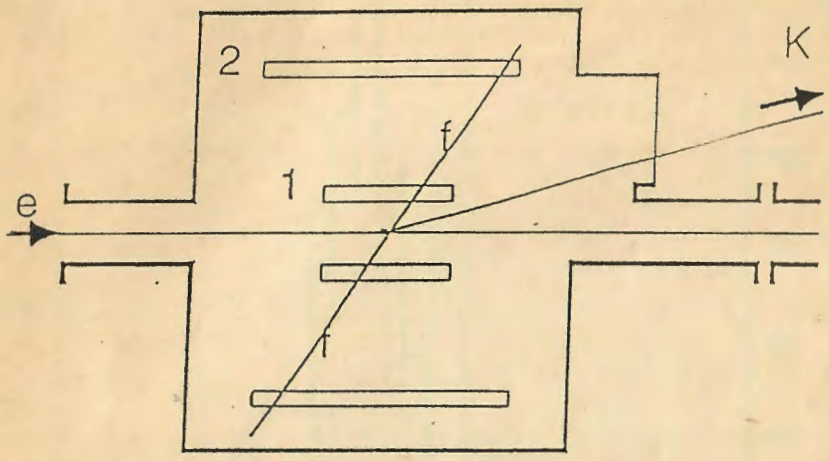

Fig.12 A schematic sketch of the time-zero FF detector.

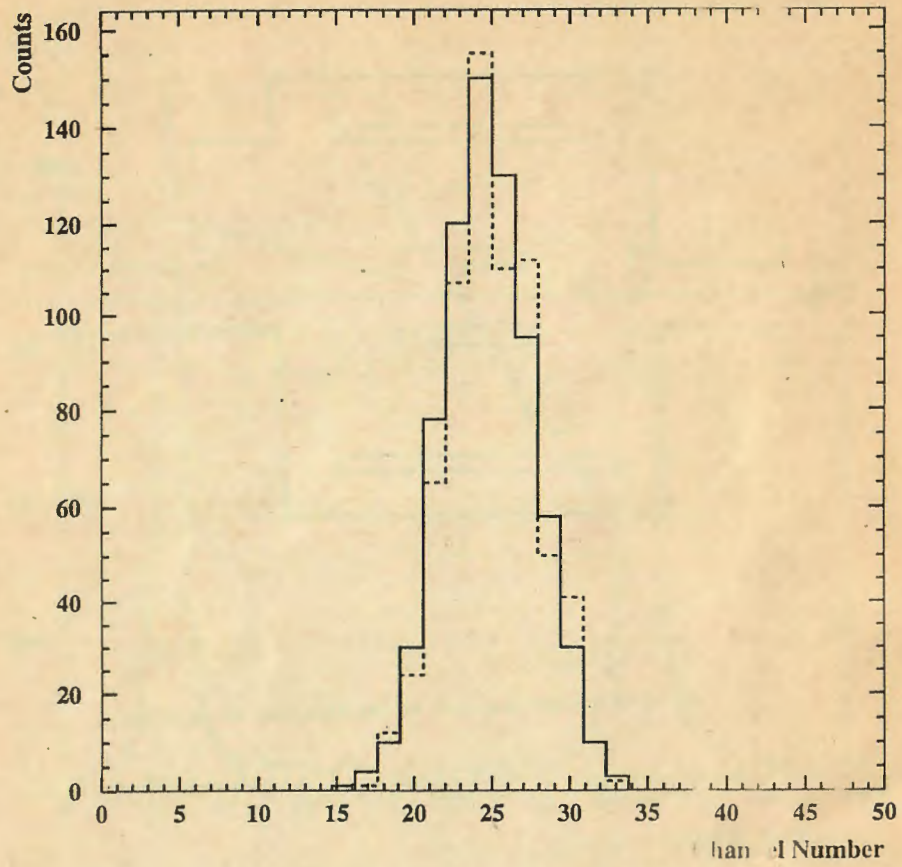

Fig.13 TOF spectrum of fragments from a ^{252}C(sou e between LPMWPCs D1 and D2 (1 ch = 11 ps) hown are the results of the measurement (lid ne) and Monte Carlo simulation (dashed l)

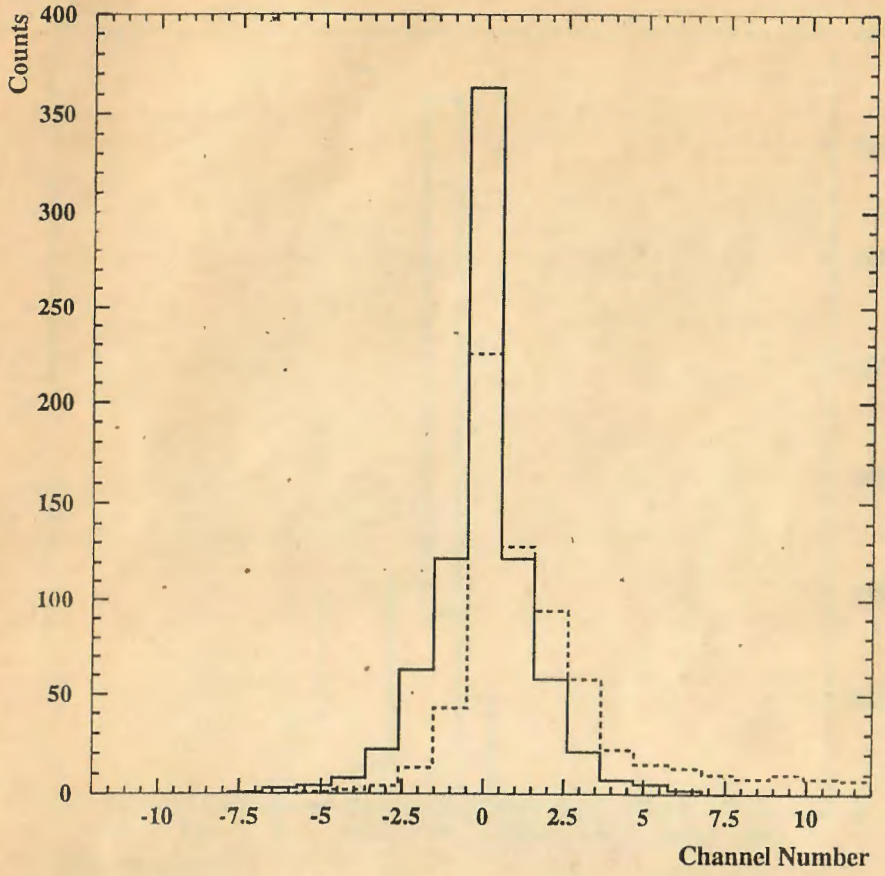

Fig.14 Monte Carlo time-zero distributions of fragments from Bi for the first chamber of time-zero FF detector(1 ch = 100 ps). The curves belong to the cases without gas(solid line) and with Hexane at 1 Torr pressure(dashed line).

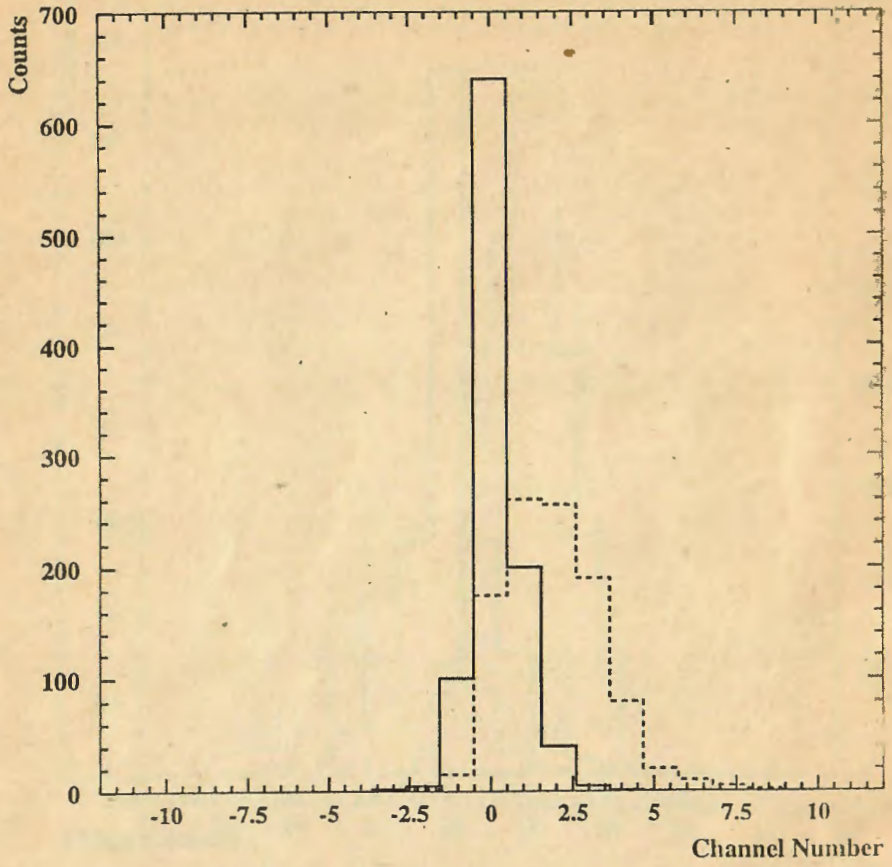

Fig.15 Monte Carlo time-zero distributions of fragments from Bi for the four chambers of the time-zero FF detector system (1 ch = 100 ps). The curves belong to the cases of delayed fission with a 200 ps liftime (dashed line) and with prompt fission (solid line).

Технический редактор А. С. Абрамян

Подписано в печать 30.10.98 Формат 64x84/16
Офсетная печать Уч. изд. л. 0,5 Тираж 50
Зак. тип. 29

Отпечатано в Ереванском физическом институте
Ереван-36 ул. Братьев Алиханян 2.